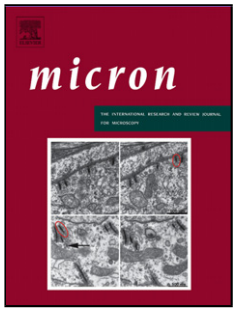

Title: On the morphology of cellulose nanofibrils obtained by TEMPO-mediated oxidation and mechanical treatment

Author: José A.F. Gamelas Jorge Pedrosa Ana F. Lourenço Peré Mutjé Israel González Gary Chinga-Carrasco Gurvinder Singh Paulo Ferreira

PII: S0968-4328(15)00016-5
DOI: http://dx.doi.org/doi:10.1016/j.micron.2015.02.003
Reference: JMIC 2162

To appear in: *Micron*

Received date: 23-12-2014
Revised date: 11-2-2015
Accepted date: 11-2-2015

Please cite this article as: Gamelas, J.A.F., Pedrosa, J., Lourenço, A.F., Mutjé, P., González, I., Chinga-Carrasco, G., Singh, G., Ferreira, P.,On the morphology of cellulose nanofibrils obtained by TEMPO-mediated oxidation and mechanical treatment, *Micron* (2015), http://dx.doi.org/10.1016/j.micron.2015.02.003

To be submitted to... . Last update 141006.

On the morphology of cellulose nanofibrils obtained by TEMPO-mediated oxidation and mechanical treatment

José A. F. Gamelas[a*], Jorge Pedrosa[a], Ana F. Lourenço[a], Peré Mutjé[b], Israel González[b], Gary Chinga-Carrasco[c], Gurvinder Singh[d], Paulo Ferreira[a**]

[a]Department of Chemical Engineering, CIEPQPF, University of Coimbra, Pólo II. R. Sílvio Lima, PT - 3030-790 Coimbra, Portugal

[b]Department of Chemical Engineering, LEPAMAP, University of Girona, c/M. Aurèlia Campmany, nº 61, Girona 17071, Spain

[c] Paper and Fibre Research Institute, PFI, Høgskoleringen 6B, N-7491, Trondheim, Norway

[d] Department of Chemical Engineering, NTNU, N-7491 Trondheim, Norway

*jafgas@eq.uc.pt (José A. F. Gamelas), Tel: 00351239798740; fax: 00351239798703

**paulo@eq.uc.pt (Paulo Ferreira), Tel: 00351239798747; fax: 00351239798703

Abstract

The morphological properties of cellulose nanofibrils (CNF) obtained from eucalyptus pulp fibres were assessed. Two samples were produced with the same chemical treatment (NaClO/NaBr/TEMPO (2,2,6,6-tetramethylpiperidine-1-oxyl radical) oxidation), but distinct mechanical treatment intensities during homogenization. It was shown that the nanofibrils production yield increases with the mechanical energy. The effect of mechanical treatment on the yield was confirmed by laser profilometry of air-dried nanocellulose films. However no significant differences were detected regarding the nanofibrils width as measured by atomic force microscopy (AFM) of air-dried films. On the other hand, differences in size were found either by laser diffraction spectroscopy or by dynamic light scattering (DLS) of the cellulose nanofibrils suspensions as a consequence of the differences in the length distribution of both samples. The nanofibrils length of the more nanofibrillated sample was calculated based on the width measured by AFM and the hydrodynamic diameter obtained by DLS. A length

value of ca. 600 nm was estimated. The DLS hydrodynamic diameter, as an equivalent spherical diameter, was used to estimate the CNF length assuming a cylinder with the same volume and with the diameter (width) assessed by AFM. A simple method is thus proposed to evaluate the cellulose nanofibrils length combining microscopy and light scattering methods.

Keywords: Nanofribrillated cellulose; TEMPO-oxidised cellulose nanofibrils; morphology; size; dynamic light scattering, atomic force microscopy

Introduction

In the last decade the interest in cellulose nanofibrils (CNF) increased exponentially. This material, usually obtained as a viscous gel, was firstly produced in the eighties (Turbak et al., 1983) after passing a wood fibre suspension several times through a homogenizer under high pressure. Chemically pre-treated CNF can be regarded as interconnected webs of tiny nanofibrils with diameters (D) typically of less than 20 nm and lengths (L) in the micrometer scale. The specific *D* and *L* dimensions of CNF can vary according to the pristine material and the conditions of the process used for their preparation but the aspect ratio (L/D) is in all cases very high (Gardner et al., 2008; Lavoine et al., 2012; Shinoda et al., 2012). CNF possesses a specific surface area significantly higher than that of the pristine cellulose fibres (values can reach more than 100 m^2/g (Lavoine et al., 2012)). However, the exact values have been difficult to assess. Nitrogen adsorption using BET calculation has been the most common method to determine the specific surface area but it is widely accepted that the BET values underestimate the real values of surface area, because the measurement is made on the material after drying, where the microfibrils are strongly aggregated by hydrogen bonding (Lavoine et al. 2012). In addition, the BET specific surface area will be also strongly dependent on the applied drying process (air drying, freeze drying, spray drying). One of the

most important characteristics of CNF is the high strength property, commonly measured on CNF films, that is the result of a high specific surface area for hydrogen bonding. Besides, highly translucent films can be obtained from the CNF suspensions. All these characteristics of CNF, namely the viscosity properties of the CNF gel, the high specific surface area, high mechanical resistance and high light transmittance of its solid films make it appealing for a wide range of applications. Just to mention a few, it may be used in formulations as a viscosity modifier, as gel for biomedical applications (Chinga-Carrasco and Syverud, 2014), as a mechanical reinforcement material in composites, including paper (Ahola et al., 2008a; Syverud and Stenius, 2009), for paper coating (Brodin et al., 2014), in films for food packaging (Syverud and Stenius, 2009; Aulin et al., 2010) and for electronic devices (Chinga-Carrasco et al., 2012), and as gas barrier material (Fukuzumi et al., 2009, Lavoine et al. 2012).

The assessment of the physical and chemical properties of cellulose nanofibrils produced by several methods is of main interest from both the fundamental and practical point of view. Accordingly to a previous review, the main points that should be addressed are the amount of produced nanomaterial, the rheology of the dispersion, the particle size (including aspect ratio) and size distribution, crystallinity, specific surface area, surface charge and chemistry, and mechanical properties (Kangas et al., 2014). Obviously, in account for the foreseen applications, some of the properties can have more importance than the others.

The size and size distribution of nanofibrils is always an important parameter to consider, but it should be mentioned that presently no standard methods or validated techniques are available for the size evaluation of polydisperse nanomaterials with a high aspect ratio (Fraschini et al., 2014). Microscopy techniques, such as high-resolution scanning electron microscopy (SEM), transmission electron microscopy (TEM) and atomic force microscopy (AFM) are most appropriate to visualize the cellulose nanofibrils (Chinga-Carrasco et al., 2014). However, it is widely recognised that these are much dependent on the operator and

are usually restricted to the analysis of a small amount of sample, besides being time-consuming (Fraschini et al., 2014). On the other hand, techniques based on light scattering, such as dynamic light scattering (DLS), can circumvent most of the drawbacks mentioned for microscopy-based techniques provided that the particles are spheres or have a shape close to that of spheres. This is not the case of cellulose nanofibrils that are closer to a cylindrical shape. Notwithstanding, it was reported for cellulose nanocrystals that the equivalent hydrodynamic radius, measured by DLS, did not differ much from the theoretical hydrodynamic radius, calculated for cylinder-shaped particles based on the dimensions of length and width assessed by Field emission-SEM (Fraschini et al. 2014). Thus, microscopy and light scattering methods are considered complementary.

In the present work, cellulose nanofibrils obtained by TEMPO-mediated oxidation and different intensity of mechanical treatment will be assessed using complementary techniques, covering structures from the micrometre to the nanoscale. Special emphasis will be put on the determination of the cellulose nanofibrils length using DLS and AFM data and different computing approaches.

Experimental section

Nanofibrils preparation

A bleached eucalyptus kraft pulp was pre-treated with NaClO and catalytic amounts of TEMPO (2,2,6,6-tetramethylpiperidine-1-oxyl radical) and NaBr according to a methodology described elsewhere (Saito et al. 2007). In a typical experiment, 15 g of cellulose fibres were dispersed in distilled water containing TEMPO (0.016 g per g of fibres) and NaBr (0.1 g per g of fibres) at a consistency of 1%. The mixture was stirred during 15 minutes at room temperature in order to assure a good dispersion of all the substances. After this, a 15% sodium hypochlorite solution was added drop by drop to the slurry. The volume of NaClO

was calculated to have 4 mmol per gram of cellulose. The pH was kept at 10 by addition of drops of a 0.5 M NaOH solution. The oxidation was considered finished when the pH kept constant at 10. The oxidized fibres were then filtered and washed with distilled water. The fibres were then passed through a homogenizer (GEA Niro Soavi Panda Plus 2000, Italy) 5 times at 300 bar (CNF-5p) or 15 times (five passes at 300 bar and 10 passes at 600 bar) (CNF-15p). Homogenization was performed at room temperature with a pulp consistency of 1.5 %. During the homogenization it is normal that after several passes the temperature of the fluid raises up to 60-70ºC. When this happened, homogenization was stopped in order to avoid pump cavitation and the process continued after cooling of the fluid and equipment at room temperature. The resulting nanofibrils were then characterized for their morphology properties, as described below.

Characterization methods

The yield of nanofibrils production was determined in triplicate after centrifugation (Alila et al. 2013) of 40 mL of CNF suspensions (0.2%, w/w) at 9000 rpm for 30 min: the retained fraction was analysed for its solid content and compared to the original to obtain by difference the percentage (w/w) of supernatant material. The percentage of fibrillar material separated at the supernatant by centrifugation, corresponds thus to the "yield". The transmittance of CNF suspensions (0.1%, w/w) in the 400-800 nm visible range was measured using a Jascow V550 spectrophotometer. Transmittance was measured immediately after stirring the CNF suspensions.

Field emission-SEM, AFM micrographs and laser profilometry (LP) were taken on CNF films. The films were obtained by air drying of the original nanocellulose suspensions (0.2%, w/w) in a Petri plate at room temperature for about 7 days.

136 The Field emission-SEM images were acquired at 1000x magnification with a Zeiss Ultra
137 field-emission SEM, using 3 kV and 4.7 mm acceleration voltage and working distance,
138 respectively.

139 AFM imaging was performed using a Multimode AFM microscope equipped with a
140 Nanoscope V controller (Digital Instruments). All images were recorded in ScanAsyst mode
141 (peak force tapping mode), at room temperature, in air. The AFM tips, of spring constant
142 value ~0.4 N/m, were purchased from Bruker AFM probes. The size of the assessed areas was
143 2 μm × 2 μm. The nanofibril diameter distribution was quantified on the AFM images, as
144 previously described by Chinga-Carrasco et al. (2011).

145 For LP analysis, samples of 10 mm × 10 mm were coated with a layer of gold (Lehmann,
146 Lehman Mess-Systeme AG, Baden-Dättwil, Germany). Ten topography images were
147 acquired from the top and bottom sides (bottom refers to the part of the film that during the
148 film formation has been in physical contact with the Petri plate and top refers to the side of
149 the film formed in contact with air). The lateral and z-resolution of the profilometry system
150 was 1 μm and 10 nm, respectively. The size of the local areas was 1 mm × 1 mm. The
151 surfaces were horizontally levelled. The surface images were bandpass filtered to suppress the
152 surface structures with wavelengths larger than approximately 160 μm, applying a FFT filter
153 implemented in the ImageJ program. The roughness described by the root-mean square (Sq)
154 was thus quantified at wavelengths of less than 160 μm (Chinga-Carrasco et al. 2014).

155 Laser diffraction spectroscopy (LDS), which is appropriate to analyze particles with size
156 larger than 1 μm, according to the Lorentz-Mie theory (Gouesbet and Grehan, 1999), was
157 performed using a Mastersizer 3000 (Malvern Instruments). 100 mL of the original CNF
158 suspensions with a dry matter-content of approximately 0.1% were prepared and magnetically
159 stirred during one hour before the measurements. The suspensions were analysed prior to
160 centrifugation, thus including all the material obtained after the chemi-mechanical treatment

of the pulp fibres. A certain volume of the prepared suspension was added to 700 mL of water in the equipment vessel until a 10–20% obscuration was reached, and the tests were performed setting the pump speed to 2000 rpm. The results presented are an average of six measurements.

Dynamic light scattering (DLS) measurements were made using a Zetasizer Nano ZS (Malvern Instruments). This technique allows the analysis of particles in the size range between 0.6 nm and 6.0 μm. The detection was made at a scattering angle of 173º and the intensity size distributions were obtained from analysis of the correlation function using the CONTIN algorithm in the instrument software. The supernatants obtained after centrifugation of 40 ml of the CNF suspensions (0.2% w/w) at 9000 rpm for 30 min were analysed, and the results were an average of five replicated measurements. Zeta potential measurements were carried out in triplicate using the same equipment.

A systematization of the part of the analysed CNF sample, the evaluated property and the technique used for that is presented in Table 1.

Table 1. The properties of CNF assessed, the different used techniques, and the part of the sample considered for analysis

Part of the analysed sample	Property	Technique
All	Light transmittance	Spectrophotometry
	Surface morphology	Field emission-SEM
		Atomic Force Microscopy
		Laser profilometry
	Particle size	Laser diffraction spectroscopy
Supernatant	Yield	Gravimetric analysis
	Particle size	Dynamic light scattering
	Particle charge	Zeta potential measurement

Results and discussion

General characterization of CNF

182

183 Two samples of cellulose nanofibrils were produced using the same TEMPO-mediated
184 oxidation pre-treatment but different extents of the subsequent mechanical treatment in a
185 homogenizer. Before the evaluation of nanofibrils size and surface properties, the suspensions
186 were characterized for the yield of nanofibrils production, zeta potential and transmittance
187 (Table 2). The zeta potential values of the two samples (-41 and -46 mV, for CNF-5p and
188 CNF-15p, respectively) are both negative and of similar magnitude. The negative values are
189 mostly due to the presence of carboxylates (COO^-) at the surface of nanofibrils generated
190 during the oxidative pre-treatment with NaClO/NaBr/TEMPO.
191 As expected, the yield of the nanofibrils sample obtained after 15 passes (95%) was much
192 higher than that obtained after 5 passes (63%), in agreement with the higher intensity of the
193 mechanical treatment. The visible spectra in the transmittance mode (Fig. 1) also evidenced
194 higher transmittance for CNF-15p, corresponding to a clearer suspension and corroborating
195 the higher amount of nanosized material in this dispersion.
196

197 **Table 2**. Results on the production of cellulose nanofibrils by TEMPO-mediated
198 oxidation

Sample	Yield (%)	Zeta Potential (mV)	Transmittance (600 nm, %)
CNF-5p	63±3	-41±4	23
CNF-15p	95±1	-46±3	56

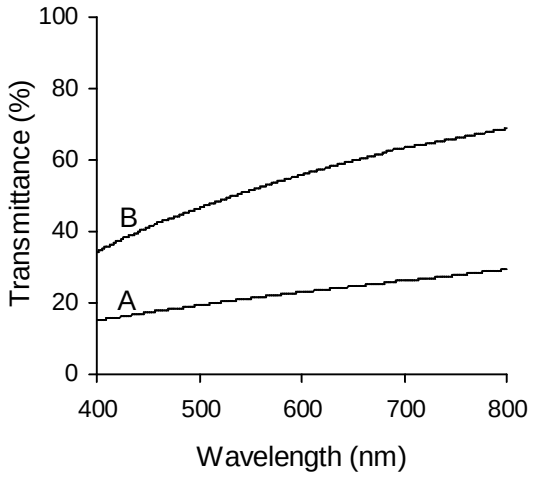

Fig. 1. Visible spectra in the transmittance mode of 0.1% suspensions of CNF-5p (A) and CNF-15p (B).

Surface morphology of CNF films

Field emission-SEM provided an insight into the surface morphology of the CNF films and, indirectly, confirmed the relative amount of nanofibrillated material. Based on the Field emission-SEM images (Fig. 2) one can observe that the CNF-5p has a major fraction of residual fibres. The amount of residual fibres was reduced in the CNF-15p sample due to the additional homogenization steps. These observations were corroborated by the LP analysis. The LP surface roughness (Rq) assessed at various wavelengths was significantly lower for the films containing higher amount of nanofibrils (CNF-15p) (Fig. 3). The LP-roughness of the CNF-15p sample confirms that this material is highly fibrillated and contains a major fraction of cellulose nanofibrils (Chinga-Carrasco et al., 2014; Chinga-Carrasco and Syverud, 2014). The higher homogeneity of the suspension of CNF-15p (transmittance of 56% at 600 nm, Table 2) and the corresponding higher amount of nanofibrils (yield of 95% of nanofibril production) produce relatively smooth film surfaces (Fig. 2 and 3).

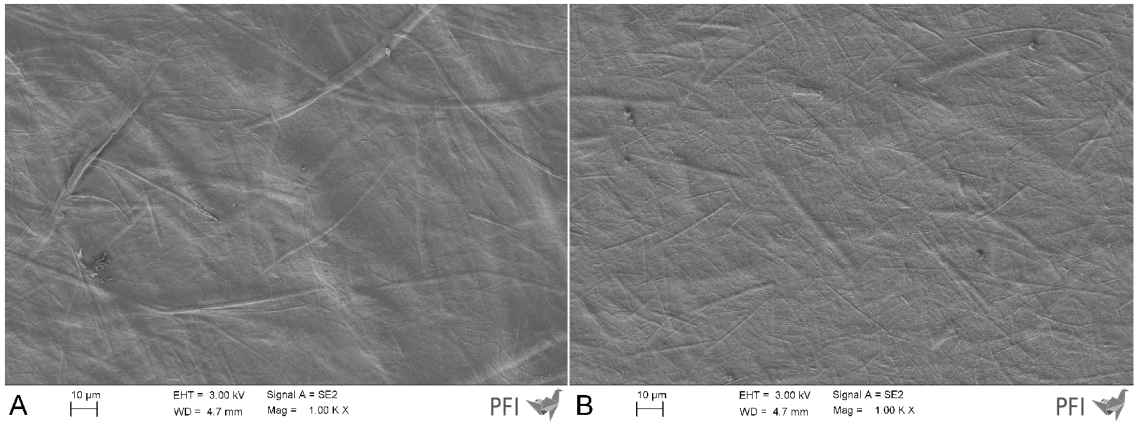

Fig. 2. Field emission-SEM of films of CNF-5p (A), and CNF-15p (B).

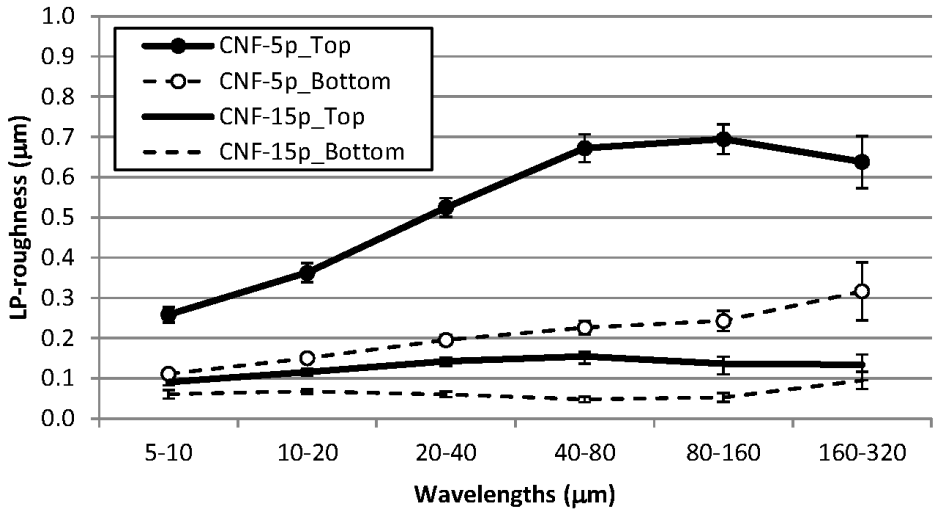

Fig. 3. Laser profilometry topography assessment (top and bottom refer to the sides of the film formed in contact with air and Petri plate, respectively)

As mentioned, AFM is a valuable technique that may be used for the assessment of the surface roughness at the nanoscale and of the cellulose nanofibrils morphology. In this work, the nanofibrils width was estimated based on AFM images of nanocellulose films (Fig. 4 and Fig. 5). A mean value of approximately 15 nm was quantified for both samples (the average width based on 4 images from each sample was 15 nm ±1.6 and 14 nm ±0.7 for CNF-5p and CNF-15p, respectively). Keep in mind that the mean value of the nanofibril widths may be

overestimated due to the AFM tip size and its geometry, which lead to a broadening of the lateral dimensions of the nanostructures (Delvallée et al., 2013). However, when comparing CNF-15p with CNF-5p and based on the SEM, LP and AFM assessments it seems evident that the mechanical treatment has a major effect on fibrillating the cellulose fibres into nanofibrils with a homogeneous size distribution.

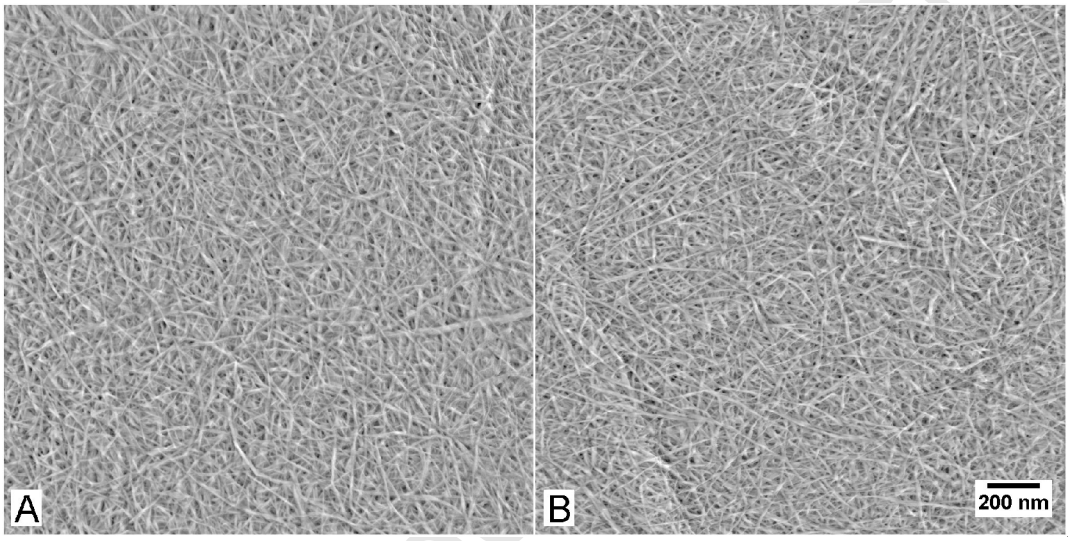

Fig. 4. AFM images of air-dried films of CNF-5p (A) and CNF-15p (B).

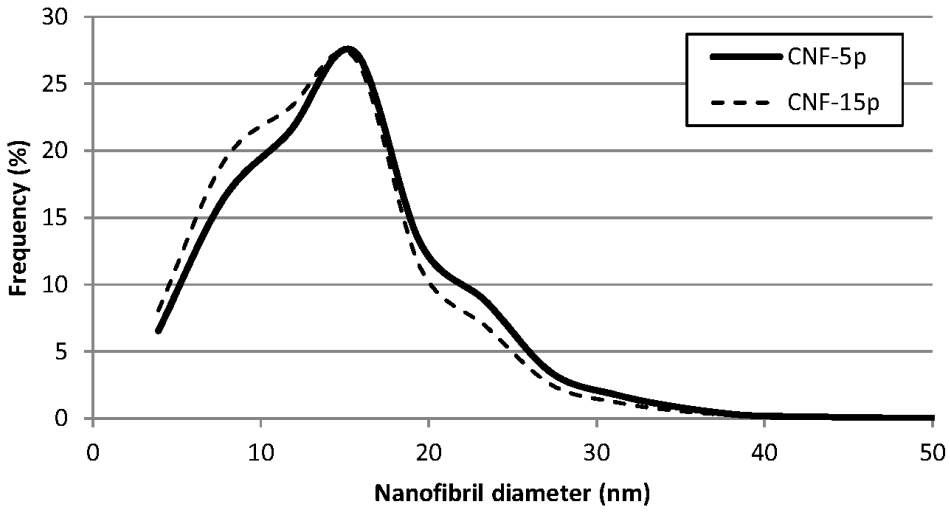

241

242 **Fig. 5.** Nanofibril diameter distribution obtained by AFM for samples CNF-5p and CNF-
243 15p.

244

245 *Complementary optical methods for the assessment of nanofibril biometry*

246 Microscopy based techniques such as AFM but also SEM and TEM are adequate to assess
247 the morphology of cellulose nanofibrils and hence they have been widely used (e.g. Saito et
248 al., 2006; Ahola et al., 2008b; Pääkkö et al., 2007; Abe et al., 2007; Fukuzumi et al., 2009;
249 Chinga-Carrasco et al., 2011). However, as mentioned in the introduction section, they may
250 be time-consuming (sample preparation, image acquisition and analysis), operator dependent
251 and restricted to the analysis of a small amount of sample. These drawbacks are particularly
252 relevant for the measurement of the nanofibrils length, which presents usually a broad
253 distribution and, besides, cannot be evaluated in images like those of Fig. 4. Therefore, in this
254 study, an attempt was made to use relatively simple and fast methods to assess the length of
255 the cellulose nanofibrils. For that, laser diffraction spectroscopy (LDS) and particularly
256 dynamic light scattering (DLS) measurements were employed. The latter has been used for
257 nanofibrils of distinct origins, as detailed in the open literature (Mandal and Chakrabarty,
258 2011; Qua et al, 2011; Beck et al. 2012; Zhou et al, 2012; Morais et al. 2013; Boluk and
259 Danumah 2014; Fraschini et al. 2014).

260

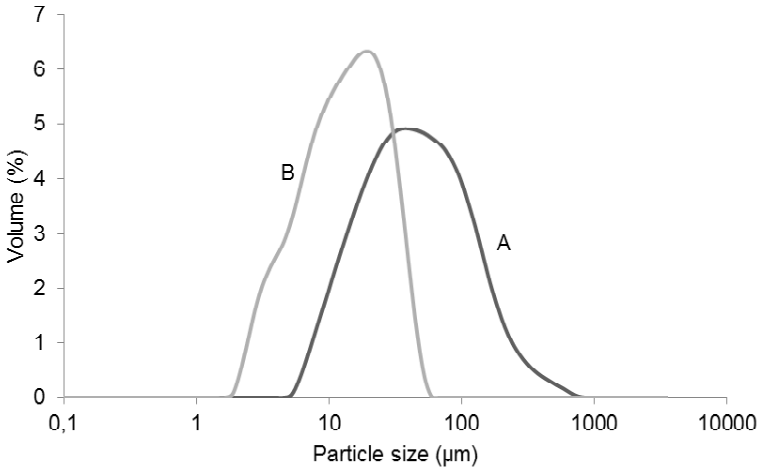

Fig. 6. Volume distributions obtained by laser diffraction spectroscopy for samples CNF-5p (A) and CNF-15p (B).

As for the laser diffraction spectroscopy, it is more convenient to particles in the micrometer range, which is not really the case of the cellulose nanofibrils in this study. However, taking into account that the produced nanofibrils suspensions also show some non-completely fibrillated content (as suggested by the yield of the production process), this technique was employed to detect and analyse the fraction of the larger material as well as of the nanofibrils aggregates (> 1 µm). The particle size distributions obtained by LDS for CNF-5p and CNF-15p are shown in Fig. 6. It should be noted that these are volume (and not number) distribution curves and therefore even the presence of a small number of less-fibrillated material and nanofibrils aggregates has a great impact on the size distribution. As clearly shown in Fig. 6, the volume distribution of the CNF-5p sample is shifted to higher size values. This may be attributed to the higher amount of less-fibrillated material presented in CNF-5p (see Table 2, Fig. 2 and Fig. 3). Moreover, it is important to note that LDS provides an equivalent diameter based distribution assuming that the light scattering pattern of the material is identical to that of spherical particles. For micro- and nano-fibrils with a high aspect ratio, this approach leads to values that can be used only for the comparison between

280 samples and not as a direct measure of the real size of the material. With this in mind, the size
281 reduction from CNF-5p to CNF-15p (Fig. 6) is obvious, when these samples are analysed as a
282 whole (i.e., without any further step of fraction selection such as centrifugation).

283 Considering the existence of nanofibrillated material, dynamic light scattering was used
284 since it is more appropriate than LDS to assess particle sizes in the nanoscale range. To get
285 more information on the produced nanofibrils size, suspensions of CNF-5p and CNF-15p
286 were centrifuged (in the same way as that used to determine the nanofibril yield) and only the
287 supernatants were analysed. The size distributions of the supernatants are depicted in Fig. 7.

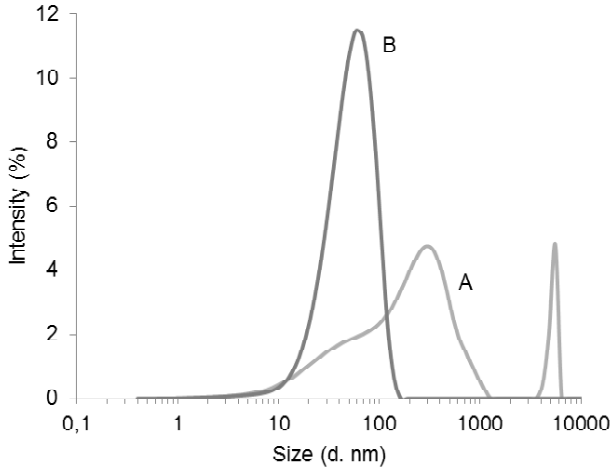

288

289 **Fig. 7**. Intensity distributions obtained by dynamic light scattering for supernatants obtained
290 after centrifugation of CNF-5p (A) and CNF-15p (B).

291

292 While sample CNF-15p presents an unimodal distribution with a mode at *ca.* 55 nm, the
293 sample CNF-5p presents a broad range of sizes from about 5 nm to 1000 nm and some objects
294 around 5000 nm. The DLS distribution of CNF-15p is more in agreement to what is expected
295 for a highly nanofibrillated material (Mandal and Chakrabarty, 2011; Zhou et al, 2012;
296 Fraschini et al. 2014). From these results, it is evident that the supernatant of sample CNF-15p
297 presents a greater uniformity in size distribution comprising only nanofibrils. The supernatant

of CNF-5p, on the other hand, still denotes some residual fibres (or nanofibrils aggregates) of higher dimension, in spite of the preliminary centrifugation process.

Due to the lack of homogeneity and broad size range observed for CNF-5p, it is not possible to relate the corresponding results obtained by DLS and AFM, contrary to the case of the CNF-15p sample. For the latter, that shows a simple size distribution, several attempts were made to obtain the length (L) of the nanofibrils by combining the DLS and AFM data, *i.e*, by considering the hydrodynamic diameter (mode) of 56 nm measured on the supernatant by DLS (D_{DLS}) and the average width of 14 nm measured on the films by AFM (W_{AFM}). In a first approach, the Tirado and Garcıa de la Torre formula for the ratio D_{HC}/D_{HS}, given by Eq. 1, was considered (Tirado and García de la Torre, 1980; Fraschini et al., 2014). Here, D_{HC} and D_{HS} are the hydrodynamic diameters, respectively, of a cylinder and a sphere, having the same volume; the term γ is defined in Eq. 2. Taking $D_{HC} = D_{DLS}$, $W = W_{AFM}$ and $D_{HS} = (3/2W^2L)^{1/3}$, an average nanofibril length (L) of 150 nm was obtained by solving the Eq. 1. However, to apply the formula described by Eq. 1, the aspect ratio of the cylinder should be between 2 and 20 which may not be the present case (Lavoine et al. 2012). Thus, the calculation of the length was also done using a formula developed for a wider range of aspect ratios (up to 100) (Hansen, 2004). The result obtained was the same (L=150 nm).

$$\frac{D_{HC}}{D_{HS}} = \frac{\left(\frac{2}{3}\right)^{1/3}\left(\frac{L}{W}\right)^{2/3}}{\ln\left(\frac{L}{W}\right)+\gamma} \qquad \text{Eq (1)}$$

$$\gamma = 0.312 + 0.565\left(\frac{W}{L}\right) - 0.100\left(\frac{W}{L}\right)^2 \qquad \text{Eq (2)}$$

In a second approach, a very simple calculation was carried out considering the mode of the intensity distribution obtained by DLS as an equivalent spherical diameter and using it to

compute the volume of the nanofibrils and deriving the length of a cylinder with the same volume and with a width assessed by AFM, as shown in Equations 3 and 4. Note that the main difference between the two approaches is that in the first approach the hydrodynamic diameter obtained by DLS is taken as a cylinder hydrodynamic diameter (D_{HC}) while in the second approach it is considered as an equivalent spherical diameter (D_{HS}). Using the second approach a value of 597 nm was obtained for L. This value is consistent with the lengths determined by TEM of TEMPO-oxidised cellulose nanofibrils having similar production yield (>95%) (Fukuzumi et al., 2013) or produced with the same amount of NaClO (4 mmol per gram of cellulose) (Shinoda et al., 2012). For instance, the latter authors obtained a number average length of 658 nm for CNF. As for the other calculated values of L, they seem too low for nanofibrils, unless only the shortest nanofibrils are being evaluated. Note also the nanofibril lengths observed in Fig. 4 (AFM images). Although it is difficult to quantify the length due to the entanglement of the nanofibril network, it can be observed that the lengths are at least >500 nm which gives supportive evidence for our proposed approach. Additionally, as stated above the AFM tip overestimates the nanofibrils width, which implies that the lengths are most probably larger than the value estimated in this study. A more accurate measure of nanofibril width could be undertaken with TEM, which will be explored in a future comparative study.

$$\frac{\pi}{6}(D_{DLS})^3 = \frac{\pi}{4}(W_{AFM})^2 L \qquad \text{Eq (3)}$$

$$L = \frac{2}{3}\frac{(D_{DLS})^3}{(W_{AFM})^2} \qquad \text{Eq (4)}$$

In summary, although different methods were used, some uncertainty remains regarding the real length of the produced nanofibrils. Note that the real length is difficult to assess by dynamic light scattering much due to the high aspect ratio of CNF. Notwithstanding, dynamic

light scattering of the supernatants of nanofibrils suspensions can be considered as a valuable tool to compare the nanofibrils size in terms of relative size trends among a series of preparations. In the case of high yields of produced nanofibrils, the values measured may provide an approximate estimate of nanofibril lengths.

Conclusions

Several methods were applied for the analysis and differentiation of CNF obtained by NaClO/NaBr/TEMPO pre-oxidation and mechanical treatment with 5 and 15 passes in a homogenizer, namely CNF-5p and CNF-15p. CNF-15p when compared to CNF-5p showed higher nanofibrils yield and correspondingly higher transmittance in the visible range, while zeta potential was similar due to the same applied chemical oxidation pre-treatment. The width of produced nanofibrils, as assessed by AFM on air-dried films was also similar. On the other hand, surface roughness of the air-dried CNF films increased for the less nanofibrillated cellulose.

Techniques different from the conventional microscopic ones to assess nanofibrils size were attempted. Laser diffraction spectroscopy, which is more appropriate to evaluate particles in the micrometer range, showed that the CNF suspension with lower fibrillated content had a volume distribution shifted to higher size value. From the size distributions measured by dynamic light scattering of the supernatants obtained from centrifugation of CNF it was evident that the supernatant of sample CNF-15p presents a greater uniformity in size distribution and only shows nanofibrils.

Using the cellulose nanofibrils width measured on the air-dried CNF films by AFM and the hydrodynamic diameter measured on the supernatant by DLS, it was possible to estimate

368 the nanofibrils length for CNF-15p. Combining microscopy and light scattering data, the
369 average length was thus calculated to be of ca. 600 nm.
370
371 **Acknowledgments**
372 The authors acknowledge QREN (Quadro de Referência Estratégico Nacional) for financial
373 support (QREN 34169 NMC). Part of this work has been supported by the Research Council
374 of Norway through the NANO2021 program, grant no. 219733 – NanoHeal: Bio-compatible
375 cellulose nanostructures for advanced wound healing applications.
376
377 **References**
378 Abe, K., Iwamoto, S., Yano, H., 2007. Obtaining cellulose nanofibers with a uniform width of
379 15 nm from wood. Biomacromolecules 8, 3276-3278.
380 Ahola, S., Österberg, M., Laine, J., 2008a. Cellulose nanofibrils – adsorption with
381 poly(amideamine) epichlorohydrin studied by QCM-D and application as a paper strength
382 additive. Cellulose 15, 303–314.
383 Ahola, S., Salmi, J., Johansson, L.-S., Laine, J., Österberg, M., 2008b. Model films from
384 native cellulose nanofibrils. Preparation, swelling, and surface interactions.
385 Biomacromolecules 9, 1273-1282.
386 Alila, S., Besbes, I., Rei Vilar, M., Mutjé, P., Boufi, S., 2013. Non-woody plants as raw
387 materials for production of microfibrillated cellulose (MFC): A comparative study. Industrial
388 Crops and Products 41, 250-259.
389 Aulin, C., Gällstedt, M., Lindström, T., 2010. Oxygen and oil barrier properties of
390 microfibrillated cellulose films and coatings. Cellulose 17, 559–574.
391 Beck, S., Bouchard, J., Berry, R., 2012. Dispersibility in water of dried nanocrystalline
392 cellulose. Biomacromolecules 13, 1486-1494.

393 Boluk, Y., Danumah, C., 2014. Analysis of cellulose nanocrystal rod lengths by dynamic light
394 scattering and electron microscopy. J. Nanopart. Res. 16, 2174.
395 Brodin, F.W., Gregersen, O.W., Syverud, K., 2014. Cellulose nanofibrils: Challenges and
396 possibilities as a paper additive or coating material – a review. Nord. Pulp Paper Res. J. 29,
397 156-166.
398 Chinga-Carrasco, G., Yu, Y., Diserud, O., 2011. Quantitative electron microscopy of
399 cellulose nanofibril structures from Eucalyptus and Pinus radiata kraft pulp fibres.
400 Microscopy and microanalysis 17, 563-571.
401 Chinga-Carrasco, G., Tobjörk, D., Österbacka, R., 2012. Inkjet-printed silver-nanoparticles on
402 nano-engineered cellulose films for electrically conducting structures and organic transistors –
403 concept and challenges. J. Nanopart. Res. 14, 1213.
404 Chinga-Carrasco, G., Averianova, N., Kondalenko, O., Garaeva, M., Petrov, V., Leinsvang,
405 B., Karlsen, T., 2014. The effect of residual fibres on the micro-topography of cellulose
406 nanopaper. Micron 56, 80-84.
407 Chinga-Carrasco, G., Syverud K., 2014. Pretreatment-dependent surface chemistry of wood
408 nanocellulose for pH-sensitive hydrogels. J Biomaterials Applications 29, 423-432.
409 Delvallée, A., Feltin, N., Ducourtieux, S., Trabelsi, M., Hochepied, J.-F., 2013. Comparison
410 of nanoparticle diameter measurements by Atomic Force Microscopy and Scanning Electron
411 Microscopy. 16th International Congress of Metrology, 06007. DOI:
412 10.1051/metrology/201306007.
413 Fraschini, C., Chauve, G., Le Berre, J-F., Ellis, S., Méthot, M., O' Connor, B., Bouchard, J.,
414 2014. Critical discussion of light scattering and microscopy techniques for CNC particle
415 sizing. Nord. Pulp Paper Res. J. 29, 31-40.

416 Fukuzumi, H., Saito, T., Iwata, T., Kumamoto, Y., Isogai, A., 2009. Transparent and high gas
417 barrier films of cellulose nanofibers prepared by TEMPO-mediated oxidation.
418 Biomacromolecules 10, 162-165.
419 Fukuzumi H., Saito T., Isogai A., 2013. Influence of TEMPO-oxidized cellulose nanofibril
420 length on film properties. Carbohydr. Polym. 93, 172-177.
421 Gouesbet, G., Grehan, G., 1999. J Opt A-Pure Appl Op. 1, 706.
422 Hansen, S., 2004. Translational friction coefficients for cylinders of arbitrary axial ratios
423 estimated by Monte Carlo simulation. J. Chem. Phys. 121, 9111-9115.
424 Kangas, H., Lahtinen, P., Sneck, A., Saariaho, A-M., Laitinen, O., Hellén, E., 2014.
425 Characterization of fibrillated celluloses. A short review and evaluation of characteristics with
426 a combination of methods. Nord. Pulp Paper Res. J. 29, 129-143.
427 Lavoine, N., Desloges, I., Dufresne, A., Bras, J., 2012. Microfibrillated celulose – its barrier
428 properties and applications in cellulosic materials: a review. Carbohydr. Polym. 90, 735-764.
429 Mandal, A., Chakrabarty, D., 2011. Isolation of nanocellulose from waste sugarcane bagasse
430 (SCB) and its characterization. Carbohydr. Polym. 86, 1291-1299.
431 Morais, J.P.S., Rosa, M.F., Filho, M.M.S., Nascimento, L.D., Nascimento, D.M., Cassales,
432 A.R., 2013. Extraction and characterization of nanocelulose structures from raw cotton linter.
433 Carbohydr. Polym. 91, 229-235.
434 Pääkkö, M., Ankerfors, M., Kosonen, H., Nykänen, A., Ahola, S., Österberg, M.,
435 Ruokolainen, J., Laine, J., Larsson, P.T., Ikkala, O., Lindström, T., 2007. Enzymatic
436 hydrolysis combined with mechanical shearing and high-pressure homogenization for
437 nanoscale cellulose fibrils and strong gels. Biomacromolecules 8, 1934-1941.
438 Qua, E.H., Hornsby, P.R., Sharma, H.S.S., Lyons, G., 2011. Preparation and characterization
439 of cellulose nanofibrils. J. Mater. Sci. 46, 6029-6045.

Saito, T., Nishiyama, Y., Putaux, J-L., Vignon, M., Isogai, A., 2006. Homogeneous Suspensions of Individualized Microfibrils from TEMPO-Catalyzed Oxidation of Native Cellulose. Biomacromolecules 7, 1687-1691.

Saito, T., Kimura, S., Nishiyama, Y., Isogai, A., 2007. Cellulose nanofibrils prepared by TEMPO-mediated oxidation of native cellulose. Biomacromolecules, 8, 2485-2491.

Shinoda, R., Saito, T., Okita, Y., Isogai A., 2012. Relationship between length and degree of polymerization of TEMPO-oxidized cellulose nanofibrils. Biomacromolecules 13, 842-849.

Syverud K., Stenius P., 2009. Strength and barrier properties of MFC films. Cellulose 16, 75-85.

Tirado, M.M., García de la Torre, J., 1979. Translational friction coefficients of rigid, symmetric top macromolecules. Application to circular cylinders. J. Chem. Phys. 71, 2581-2587.

Turbak, A. F., Snyder, F.W., Sandberg, K.R., 1983. Micro-fibrillated cellulose, a new cellulose product: properties, uses, and commercial potential. J. Appl. Polym. Sci. Appl. Polym. Symp. 37, 815-827.

Zhou, Y.M., Fu, S.Y., Zheng, L.M., Zhan, H. Y., 2012. Effect of nanocellulose isolation techniques on the formation of reinforced poly(vinyl alcohol) nanocomposite films. eXPRESS Polymer Letters 6, 794-804.

458 Highlights:

459

460 AFM and dynamic light scattering (DLS) were used for the cellulose nanofibril analysis

461 Laser diffraction spectroscopy was used to assess the less-fibrillated material

462 The length of cellulose nanofibril could be estimated based on AFM and DLS data

463 A value of ca. 600 nm was estimated for the TEMPO-oxidised cellulose nanofibril length

464
465
466
467